REPORT ASSESSMENT OF INJECTIVITY PROBLEMS IN GEOTHERMAL GREENHOUSE HEATING WELLS

10 FEBRUARY 2015

This research programme is financed by the « Programma Kas als Energiebron ».

EXECUTIVE SUMMARY

The Dutch greenhouse farming sector is making increasing use of geothermal heat as a renewable energy substitute for the burning of natural gas. The heat extraction scheme, known as the geothermal space heating doublet, combines a production well lifting, via an electrosubmersible pump (ESP) set, the hot fluid to a surface heat exchanger and where needed an injection well pumping the heat depleted brine back into the source reservoir.

During the production/injection exploitation process the geothermal fluid undergoes a series of thermodynamic-pressure, temperature – changes, which if not properly assessed and controlled may lead to severe thermochemical shortcomings. Among these, solubility losses, supersaturation and precipitation in the form of scale of sensitive, presumably carbonate, mineral species take an important share. The latter was the primarly suspected cause of the often severe injectivity decline noticed on several injector wells, which to be identified require on the spot *ad-hoc* investigations. This prompted the greenhouse farming community to launch a thorough well monitoring and fluid sampling campaign, carried out in July 2013, awarded to GPC IP (France) and KWR (The Netherlands) in order to produce relevant damage diagnosis and remedial/best practice protocols.

Within this research, GPC IP investigations concentrated on well performance and fluid physical and thermodynamic properties, while KWR concerns focused on the geochemical processes occuring in geothermal systems and deemed decisive in the damaging process.

The main problems identified on most of the sites are low pumping efficiencies, degassing and scaling. In some instances degassing occurs right in the well and two phase flow is observed.

Further to the analysis of gases and scale samples it is clear that one of the main responsible for the existence of high quantities of particles in the geothermal loop is the degassing of CO_2 which leads for instance to the precipitation of carbonates. On one site important quantities of lead carbonates were assessed.

It is concluded that the main cause for accumulation of minerals on filters and as scaling is due to the degassing of CO_2 during the rise in the production well and in subsequent parts of the geothermal system. The CO_2 degassing results from the drop in the gas pressure that is maintained at reservoir depth (hydrostatic pressure) to the relatively low pressure at which the geothermal system at the surface are operated. The loss of CO_2 results in subsequent precipitation of carbonate minerals.

Depending on the chemical composition of the geothermal water in the reservoir, Ca-rich, Fe-rich or Pb-rich carbonates were preferentially precipitated, as was confirmed by analysis of filter and scaling accumulates from various systems.

Among the candidate remedial alternatives, to be implemented further to a thorough-site specific-damage diagnosis and well status, ought to be mentioned:

(i) higher (above bubble point) production wellhead pressures, whenever allowed by heat exchanger service pressures, as practiced actually on two doublets;

(ii) well stimulation using either organic (acetic, EDTA...) or mud (HCl + HF) acids;

(iii) submersible pump (ESP) vortex separators;

(iv) downhole chemical injection lines of scaling inhibitors, designed further to pilot tests on geothermal fluids sampled downhole, and

(v) last but not least pressure sustained $C0_2$ injection. Actually, since degassing of CO_2 pressure acts as the main driver for the carbonate precipitation observed, CO_2 pressure control also provides a solution. Luckily, since CO_2 appears to only represent a relatively small fraction of the total gas pressure in the geothermal reservoirs studied, only a limited level of CO_2-dosing is required to prevent or re-dissolve carbonate precipitates. The required partial CO_2 pressure seems well achievable within the operational pressures currently maintained in the geothermal systems. For sites with lead carbonate precipitation, an increased CO_2 pressure is required to compensate for the decrease of lead carbonate solubility with lower temperatures.

CONTENTS

LIST OF FIGURES

LIST OF TABLES

1. INTRODUCTION

The Dutch greenhouse farming sector is making increasing use of geothermal heat as a renewable energy substitute for the burning of natural gas. The heat extraction scheme, known as the geothermal space heating doublet, combines a production well lifting, via an electrosubmersible pump (ESP) set, the hot fluid to a surface heat exchanger and an injection well pumping the heat depleted brine back into the source reservoir. The geothermal fluid, a hot saline, slightly acid, brine including a methane rich solution gas phase and, occasionally, traces of crude oil is hosted in dominantly clastic (sandstone) and, in one instance, carbonate (limestone, dolomite) sedimentary rocks.

During the production/injection exploitation process the geothermal fluid undergoes a series of thermodynamic-pressure, temperature-changes, which if not properly assessed and controlled may lead to severe thermochemical shortcomings. Among these, solubility losses, supersaturation and precipitation in the form of scale of sensitive, presumably carbonate, mineral species take an important share. The latter was the primarly suspected cause of the often severe injectivity decline noticed on several injector wells, which to be identified require on the spot *ad-hoc* investigations. This prompted the greenhouse farming community to launch a thorough well monitoring and fluid sampling campaign, awarded to GPC IP and KWR in order to produce relevant damage diagnosis and remedial/best practice protocols.

The forthcoming report campaign results, findings on impairment driving mechanisms and, last but not least, damage removal and preventing recommendations.

2. METHODOLOGY

An extensive monitoring campaign, jointly implemented by GPC IP and KWR, has been carried out in July 2013 on the site locations documented in Table 1. It consisted of the following field measurements and fluid sampling operated at wellheads and eventually at degasser vessel outlet.

- water sampling at production and injection wellheads
- solution gas sampling on production wellheads and on the online gas stripping facility whenever installed
- water physicochemical measurements
- resource hydrothermal and thermodynamic properties
- pump performance
- well deliverability/injectibility

Table 1 : Tested and sampled wells information

OPERATOR	LOCATION	FORMATION
Californië Wijnen Geothermie	Californië (Grubbenvorst)	Carboniferous
Van den Bosch	Berkel	Rijswijk
Van den Bosch	Bleiswijk	Rijswijk
Ammerlaan	Pijnacker	Rijswijk+Delft sandstones
Gebr. Duijvestijn	Pijnacker	Rijswijk+Delft sandstones
Greenwell	Honselersdijk	Rijswijk+Delft sandstones
ECW	Middenmeer	Slochteren
Greenhouse Geo Power	Koekoekspolder	Slochteren
Floricultura	Heemskerk	

2.1. Well and reservoir assessments

The measures listed hereunder prefigure the content of a future space/heating doublet monitoring protocol.

2.1.1. Production and injection well hydrothermal and electrical measurements

They aim at assessing resource attributes, well performance, pumping equipment efficiencies and ultimately well deliverability/injectibility.

2.1.2. Production wellhead water and gas sampling

They address (i) water electrochemical parameters pH, Redox potential, conductivity, (ii) solution gas phase bubble point pressure, and gas liquid ratio, and (iii) distributions of solid particle suspensions completed via millipore staged filtration indicative of liquid turbidity and internal particles entrainment.

pH and conductivity are measured via portable WTW meters and Redox potential by Platinium electrodes. On site (well head) bubble point (BP) and gas liquid ratio (GLR) are determined by the outfit (degassing vessel and gas trap) described in Figure .

Note that none of the solution gas properties have been derived from PVT analysis on bottomhole samples.

As a result the site 1 PVT results added *in fine* ought to be regarded as an exception before becoming hopefully a future routine practice.

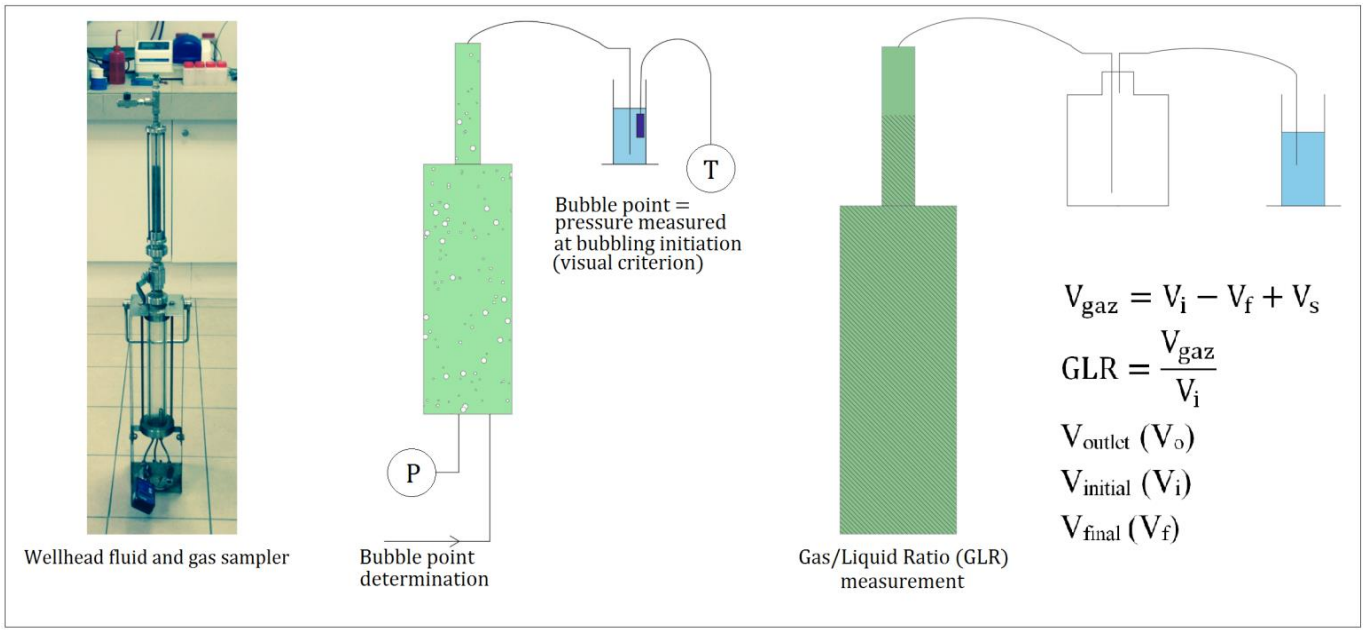

Figure 1 : Bubble point and fluid sampling field outfit

2.2. Water sampling and field measurements

An extensive measurement campaign consisting in water and gas sampling, electrical measurements, doublet diagnosis has been carried out in July 2013. This programme was jointly implemented by KWR and GPC IP and consisted in:

- *water sampling* on production and injection wells
- *solution gas sampling* on production wells, complemented on the latter by the online gas stripping facility (whenever installed).
- *physicochemical measurements* of water pH, Eh and electrical conductivity at well heads.
- *well step drawdown tests* in order to derive the well head pressure vs flowrate characteristic curve, along control of associated electric equipment (ESP transformer, frequency converter) of both production and injection wells.

Within this work programme GPC focused on the well related aspects, while KWR focused on the (geo)chemical processes that occur in the geothermal systems.

2.3. Chemical analysis

On the same day of sampling, the samples taken were transferred to the various laboratories. The storage period was kept to a minimum and analysis was performed within a few days.

2.3.1. Water analyses

Water compositions were determined by wet chemical analysis (Table 2). For the cations and trace elements were performed with ICP-MS on after total destruction using HNO_3 without and after filtration (0.45m). Anions were analyzed using ion chromatography (HCO_3, Cl, SO_4, F). Separate analyses were performed for NH_4, PO_4, sulfide, and silica content. Microbiological analyses were performed for microbial activity and ATP biomass analysis.

Table 2: Water analyses performed on the geothermal systems studied.

SITE	WELL TESTED/SAMPLED		REMARKS
	GPC IP	KWR	
1	P, I	P, D, I	
2	P, I	P, I	
3	P, I	P, I	
4	P, I	P, I	
5	P, I	P, I	
6	P	P	
7			P (TNO)
8			P (TNO)
9			P (TNO)

The water type labels P and I indicated production and injection wells respectively. For water type D, the water between the degasser and the heat exchanger was sampled. For sites 7-9 the composition of production water was taken from the compiled data by TNO (Wasch 2014).

2.3.2. Gas analyses

The cylinders containing the pressured samples of production and injection water (Table 3) were processed by ISOLAB BV by releasing (flashing) a small part the total gas pressure into in a small headspace volume, followed by GC analysis using helium as carrier gas. Analyses were performed in triplicate. The gas composition was determined by analysing for the following gas components: N_2, CO_2, H_2S, Methane (C1, CH_4), Ethane, C_2 (Ethane), Propene, C_3 (propane), iC_4, nC_4 (n-butane), neo-C_5, iC_5, nC_5 and C_6+ (hexane and longer carbon chains). For the injection waters at sites 1 and 4, repeat analysis were performed with argon as carrier gas, to verify the presence of helium in the extracted gas.

Table 3: Sites for which the gas composition of the produced (P) and injected (I) were determined

Site			Water Type	Comment
1			P,I	
3			P,I	
4			P,I	
5			P,I	
6			P	Insufficient gas for complete analysis

2.3.3. Scale analysis

Accumulation of material is observed in several sites. Samples from material accumulated on filters or as scaling were collected from three sites (Table 4). Analysis was performed after total destruction using HNO_3, followed by the same inorganic elemental analysis as described for the water samples (**§ 2.3.1**).

Table 4 : Geothermal systems from which the composition of accumulations as scalant and/or in the filter was determined

Site			Type	Sample Description
1			Scalant Filter	Brown chunks on flange window Scale on stainless steel filter
5			Filter	Filter with trapped particles
7			Scalant	Slurry taken from the bottom

3. RESULTS AND DISCUSSION

3.1. Well and reservoir performance

Results displayed in tables 5 to 11 suggest the following comments.

3.1.1. Well deliverabilities and injectibilities

It can be seen from Table 5 that (i) four wells, out of the seven tested, show low productive capacities with PIs lower than 5 m^3/h/bar among which three sites are located in the western (Rotterdam area) fine grained Rijswijk/Delft sandstone reservoirs and one in the eastern site 6 fractured carbonate rocks subject to rapid, fracturing induced, productivity changes (see nearby site 6), and (ii) three (site 4, 5, 6 higher productivities (PIs > 10 m^3/h/bar) located westward (site 4, 5) and eastward site 6 respectively.

PIs in the eastern area must account for depleted static water levels at depths close to 60 mbgl, a figure which should be turned into an asset when contemplating well injectivities. This is apparently not the case as only two injector wells (site 2 and 5), out of five tested, demonstrate reasonably high injective capacities (II > 10 m^3/h/bar) whereas three (site 1, 3, 4) remain poorly injective (II < 5 m^3/h/bar). Note that all tested injector wells belong to the western sandstone reservoir.

The causes of these variations cannot be clearly identified in the absence of, bottomhole recorded, pressure build up/fall off test data and fluid sampling which would provide unvaluable information regarding well impairment (skin damage) and, PVT derived, degassing (bubble point) pressures and solution gas/water ratios.

Measurement of site 6 shall be treated with caution because production time before sampling was relatively short (few hours). KWR concluded that the short production time was sufficient to flush all resident water from the wells and stabilize the meters. So this composition should be representative for the actual water in the reservoir. Also based on the resulting water composition.

Table 5 : Well performance review

SITE / INDEX	1	2	3	4	5	6	6
Productivity Index PI (m^3/h/bar)	4.6	4.2	2.7	11	15	17	3.3
Injectivity Index II (m^3/h/bar)	2.5	13.9	3	3.2	10.5	-	-
Pumping efficiencies h(%)							
Production (ESP)	35	58/65	51	43	35	27	39
Injection	50	37	43	61	78	-	-

Table 6 : site 1 - Production/injection electrical measurements

Site 1 8/7/07/2013	8/7/07/2013 PRODUCTION	14h00 INJECTION	8/7/07/2013 PRODUCTION	11h20 INJECTION
RESOURCE CARACTERISTICS				
Flowrate (m^3/h)	82.1	82.1	68.8	68.8
Temperature (°C)	70	34	70	34
Pressure sensor depth (bars)	30.19	*	33.18	*
Dynamic water level (m bgl)	-157.2	*	-126.3	*
Production pump discharge pressure (bars)	2.8	***	2.6	***
Injection pump inlet pressure (bars)	***	4.1	***	4.8
Injection pump discharge pressure (bars)	***	30.3	***	26.0
injection pressure @ 40 °C (bars)	***	30.6	***	26.3
Production pump head (m)	186	268	154	216
CONTROL INSTRUMENTS				
Motor voltage (V)	264	*	244	*
Current intensity of the grid (A)	382/391/391	222	344/359/352	189
Frequency converter f, (Hz)	41	45.1	38.1	41.6
MEASUREMENTS				
Voltage between phases 1 et 2 (Volts)	398.7	398.7	399.6	400.2
Voltage between phases 1 et 3 (Volts)	400.3	400.7	401.2	401.8
Voltage between phases 2 et 3 (Volts)	400.4	400.3	401.2	401.8
Current intensity * phase 1 * (A)	350.1	214.8	294.5	156.8
Current intensity * phase 2 * (A)	343.1	208.2	291.2	151.8
Current intensity * phase 3 * (A)	348.2	211.7	291.4	152.9
Cosine phi grid	0.49	0.83	0.45	0.78
RENDEMENTS				
Frequency converter power (kWel)	118	122	91	83
Theoretically absorbed power (kWel)	42	60	29	41
Overall efficiency (%)	35	49	32	49
COMMENTS				
-Low efficiency of production pump -Parameters are stable -No free gas in the circuit				

Table 7 : site 4 - Production/injection electrical measurements

Site 4 July 2013	09-Jul-13 PRODUCTION	16h00 INJECTION
RESOURCE CARACTERISTICS		
Flowrate (m^3/h)	144	144
Temperature (°C)	70.39	42.53
Pressure sensor depth (bars)	30	*
Dynamic water level (m bgl)	-117.2	*
Production pump discharge pressure (bars)	1.4	***
Injection pump inlet pressure (bars)	***	2.4
Injection pump discharge pressure (bars)	***	45.2
injection pressure @ 40 °C (bars)	***	45.0
Production pump head (m)	132	438
CONTROL INSTRUMENTS		
Motor voltage (V)	*	*
Current intensity of the grid (A)	*	*
Frequency converter f, (Hz)	*	*
MEASUREMENTS		
Voltage between phases 1 et 2 (Volts)	408.7	407.9
Voltage between phases 1 et 3 (Volts)	409.9	407.3
Voltage between phases 2 et 3 (Volts)	410.4	408.0
Current intensity * phase 1 * (A)	185.2	448.8
Current intensity * phase 2 * (A)	183.5	438.6
Current intensity * phase 3 * (A)	186.5	438.6
Cosine phi grid	0.92	0.91
EFFICENCY		
Frequency converter power (kW_{el})	121	283
Theoretically absorbed power (kW_{el})	52	172
Overall efficiency (%)	**43**	**61**
COMMENTS		
-Low efficiency 43% -Stable values -Degassing acceptable -Two phase flow in the production tubing		

Table 8 : site 5 - Production/injection electrical measurements

Site 5 July 2013	10-Jul-13 PRODUCTION	15h30 INJECTION
RESOURCE CARACTERISTICS		
Flowrate (m^3/h)	107.45	107.45
Temperature (°C)	84.8	40
Pressure sensor depth (bars)	36.92	*
Dynamic water level (m bgl)	-67.5	*
Production pump discharge pressure (bars)	3.7	***
Injection pump inlet pressure (bars)	***	2.4
Injection pump discharge pressure (bars)	***	10.2
injection pressure @ 40 °C (bars)	***	10.1
Production pump head (m)	106	79
CONTROL INSTRUMENTS		
Motor voltage (V)	265	*
Current intensity of the grid (A)	383/399/384	*
Frequency converter f, (Hz)	35.4	*
MEASUREMENTS		
Voltage between phases 1 et 2 (Volts)	402.2	397.2
Voltage between phases 1 et 3 (Volts)	401.8	397.1
Voltage between phases 2 et 3 (Volts)	401.5	396.8
Current intensity * phase 1 * (A)	280.8	45.4
Current intensity * phase 2 * (A)	280.9	46.5
Current intensity * phase 3 * (A)	276.3	45.3
Cosine phi grid	0.46	0.94
EFFICENCY		
Frequency controller power (kW_{el})	89	30
Theoretically absorbed power (kW_{el})	31	23
Overall efficiency (%)	**35**	**78**
COMMENTS		
-Low efficiency of production pump -Parameters are stable -No gas in the circuit		

Table 9 : site 2 - Production/injection electrical measurements

Site 2 July 2013	09-Jul-13 PRODUCTION	16h00 INJECTION	09-Jul-13 PRODUCTION	 INJECTION
RESOURCE CARACTERISTICS				
Flowrate (m^3/h)	205	205	190	190
Temperature (°C)	60	32	60	32
Pressure sensor depth (bars)	31.08	*	34.12	*
Dynamic water level (m bgl)	-398.0	*	-366.5	*
Production pump discharge pressure (bars)	8.6	***	8.0	***
Injection pump inlet pressure (bars)	***	7.8	***	7.0
Injection pump discharge pressure (bars)	***	14.8	***	12.7
injection pressure @ 40 °C (bars)	***	15.2	***	13.1
Production pump head (m)	487	72	449	58
CONTROL INSTRUMENTS				
Motor voltage (V)	377	*	360	*
Current intensity of the grid (A)	963/950/913	174	823/903/866	174
Frequency converter f, (Hz)	52.5	50	50.3	50
MEASUREMENTS				
Voltage between phases 1 et 2 (Volts)	389.2	388.6	388.5	389.8
Voltage between phases 1 et 3 (Volts)	389.5	388.5	388.5	388.6
Voltage between phases 2 et 3 (Volts)	388.2	388.7	389.4	389.0
Current intensity * phase 1 * (A)	838.3	180.4	666.0	138.9
Current intensity * phase 2 * (A)	846.9	173.2	675.2	140.2
Current intensity * phase 3 * (A)	848.7	176.6	699.5	143.5
Cosine phi grid	0.83	0.90	0.78	0.83
EFFICENCY				
Frequency converter power (kW_{el})	469	107	357	79
Theoretically absorbed power (kW_{el})	272	40	233	30
Overall efficiency (%)	**58**	**37**	**65**	**38**
COMMENTS				
-Efficiency of production pump acceptable -Many harmonics on the injection -Parameters are stable -Production above bbp, no free gas				

Table 10 : site 3 - Production/injection electrical measurements

Site 3 July 2013	10-Jul-13 PRODUCTION	16h00 INJECTION
RESOURCE CARACTERISTICS		
Flowrate (m^3/h)	78	78
Temperature (°C)	66	32
Pressure sensor depth (bars)	21	*
Dynamic water level (m bgl)	-157.4	*
Production pump discharge pressure (bars)	13.0	***
Injection pump inlet pressure (bars)	***	12.6
Injection pump discharge pressure (bars)	***	26.0
injection pressure @ 40 °C (bars)	***	26.4
Production pump head (m)	292	137
CONTROL INSTRUMENTS		
Motor voltage (V)	254	*
Current intensity of the grid (A)	462/463/470	139
Frequency converter f, (Hz)	41	44
MEASUREMENTS		
Voltage between phases 1 et 2 (Volts)	397.5	403.4
Voltage between phases 1 et 3 (Volts)	398.4	405.1
Voltage between phases 2 et 3 (Volts)	398.8	404.4
Current intensity * phase 1 * (A)	343.2	112.7
Current intensity * phase 2 * (A)	345.8	107.1
Current intensity * phase 3 * (A)	350.1	114.7
Cosine phi grid	0.51	0.87
EFFICENCY		
Frequency converter power (kW_{el})	122	68
Theoretically absorbed power (kW_{el})	62	29
Overall efficiency (%)	**51**	**43**
COMMENTS		
-Efficiency of production pump acceptable -Many harmonics on both production and pumps injection -Parameters are stable -Production above bbp, no free gas		

Table 11 : site 6 - Production/injection electrical measurements

Site 6 July 2013	11-Jul-13 PRODUCTION	11-Jul-13 PRODUCTION
RESOURCE CARACTERISTICS		
Flowrate (m^3/h)	100	257
Temperature (°C)	57.2	60.3
Pressure sensor depth (bars)	14.6	19.38
Dynamic water level (m bgl)	-281.7	-115.2
Production pump discharge pressure (bars)	2.2	3.2
Injection pump inlet pressure (bars)	***	***
Injection pump discharge pressure (bars)	***	***
injection pressure @ 40 °C (bars)	***	***
Production pump head (m)	304	148
CONTROL INSTRUMENTS		
Motor voltage (V)	420	420
Current intensity of the grid (A)	571/571/561	911/950/924
Frequency converter f, (Hz)	59.9	60
MEASUREMENTS		
Voltage between phases 1 et 2 (Volts)	409.5	406.5
Voltage between phases 1 et 3 (Volts)	409.8	406.4
Voltage between phases 2 et 3 (Volts)	410.2	407.4
Current intensity * phase 1 * (A)	350.0	610.4
Current intensity * phase 2 * (A)	350.0	622.6
Current intensity * phase 3 * (A)	350.0	603.4
Cosine phi grid	0.85	0.89
EFFICENCY		
Frequency converter power (kW_{el})	211	384
Theoretically absorbed power (kW_{el})	83	104
Overall efficiency (%)	**39**	**27**
COMMENTS		
-Measurements shall be treated with caution because production time before sampling was relatively short (few hours). -Parameters stable	Stable measurements Low efficiency	Many particles Low efficiency

3.1.2. Pump performance

In most instances, with the sole exception of site 2 and 3, production wells exhibit poor submersible pump (ESP) efficiencies, which otherwise shape significantly lower than 50% overall (i.e. pump x motor x transformer x cable x frequency converter) system efficiency.

Three sites (site 1, 4 and 5) show elsewhere higher than 50% overall injection pump efficiencies.

Summing up, pumping equipment do not score satisfactorily. Obviously, here, optimization of pumping system design and operation should be sought in order to boost efficiencies and diminish accordingly power consumption and related OPEX costs.

3.2. Fluid physical and thermodynamic properties

Analytical results are compiled for the seven sampled in tables 12 to 18 and summarized in Table 19.

Table 12 : site 1 - Particle and gas (bbp and GWR) measurements

DATE	08-Jul-13
SAMPLING POINT	PRODUCTION
OPERATING DATA	
Flow (in m^3/h)	69
Pressure (in bars)	2.6
Temperature (in °C)	71.8
ELECTROCHEMICAL PARAMETERS	
pH @ 20°C	6.08
Potential Redox (in mV)	-276
Conductivity @ 20°C (in µS/cm)	142,500
MAJOR IONIC PHASES (mg/l)	
Chloride	77,281
SUSPENDED PARTICLES	mg/l * %
0,20 to 0,45 µm	29,30*70,4
0,45 to 1,20 µm	10,19*24,5
1,20 to 3,00 µm	0,316*0,8
3,0 to 5,0 µm	0,392*0,9
5,0 to 8,0 µm	0,515*1,2
sup. of 8,0 µm	0,890*2,1
TOTAL	41,6*100
DISSOLVED GAS PHASE	
Bubble point (bars)	>2.6
Gas/liquid ratio (%)	Measurement not possible

Table 13 : site 4 - Particle and gas (bbp and GWR) measurements

DATE	09-Jul-13
SAMPLING POINT	PRODUCTION
OPERATING DATA	
Flowrate (m^3/h)	144
Pressure (bars)	1.4
Temperature (°C)	69.1
ELECTROCHEMICAL PARAMETERS	
pH @ 20°C	6.25
Potential Redox (mV)	-267
Conductivity @ 20°C (µS/cm)	142,000
MAJOR IONIC PHASES (mg/l)	
Chloride	77,636
SUSPENDED PARTICLES	**mg/l * %**
0,20 to 0,45 µm	76,2*66,8
0,45 to 1,20 µm	36,146*31,7
1,20 to 3,00 µm	0,382*0,3
3,0 to 5,0 µm	0,277*0,2
5,0 to 8,0 µm	0,172*0,2
sup. of 8,0 µm	0,823*0,7
TOTAL	**114*100**
DISSOLVED GAS PHASE	
Bubble point (bars)	>1.4
Gas/liquid ratio (%)	Measure impossible

Table 14 : site 5- Particle and gas (bbp and GWR) measurements

DATE	10-Jul-13
SAMPLING DATA	PRODUCTION
OPERATING DATA	
Flow (m^3/h)	108
Pressure (bars)	3.7
Temperature (°C)	84.0
ELECTROCHEMICAL PARAMETERS	
pH @ 20°C	5.84
Potential Redox (mV)	-191
Conductivity @ 20°C (µS/cm)	145,500
MAJOR IONIC PHASES (mg/l)	
Chloride	84,371
SUSPENDED PARTICLES	**mg/l * %**
0,20 to 0,45 µm	12,825*53,5
0,45 to 1,20 µm	9,213*38,5
1,20 to 3,00 µm	0,003*0,0
3,0 to 5,0 µm	0,787*3,3
5,0 to 8,0 µm	0,095*0,4
sup. of 8,0 µm	1,027*4,3
TOTAL	**23,95*100**
DISSOLVED GAS PHASE	
Bubble point (bars)	>3.74
Gas/liquid ratio (%)	Measure impossible

Table 15 : site 2 - Particle and gas (bbp and GWR) measurements

DATE	09-Jul-13
SAMPLING POINT	PRODUCTION
OPERATING DATA	
Flow (m^3/h)	203
Pressure (bars)	8.6
Temperature (°C)	59.4
ELECTROCHEMICAL PARAMETERS	
pH @ 20°C	6.45
Potential Redox (mV)	-321
Conductivity @ 20°C (µS/cm)	123,900
MAJOR IONIC PHASES (mg/l)	
Chloride	62,038
SUSPENDED PARTICLES	**mg/l * %**
0,20 to 0,45 µm	8,60*54,6
0,45 to 1,20 µm	5,45*34,6
1,20 to 3,00 µm	0,322*2,0
3,0 to 5,0 µm	0,228*1,4
5,0 to 8,0 µm	0,002*0,0
sup. of 8,0 µm	1,148*7,3
TOTAL	**15,75*100**
DISSOLVED GAS PHASE	
Bubble point (bars)	8.5
Gas/liquid ratio (%)	48

Table 16 : site 3 - Particle and gas (bbp and GWR) measurements

DATE	10-Jul-13
SAMPLING POINT	PRODUCTION
OPERATING DATA	
Flow (m^3/h)	78
Pressure (bars)	13.0
Temperature (°C)	62.2
ELECTROCHEMICAL PARAMETERS	
pH brought back to 20°C	6.07
Potential Redox (mV)	-228
Conductivity @ 20°C (µS/cm)	130,900
MAJOR IONIC PHASES (mg/l)	
Chloride	67,710
SUSPENDED PARTICLES	mg/l * %
0,20 to 0,45 µm	12,65*58,2
0,45 to 1,20 µm	7,696*35,4
1,20 to 3,00 µm	0,354*1,6
3,0 to 5,0 µm	0,200*0,9
5,0 to 8,0 µm	0,148*0,7
sup. of 8,0 µm	0,702*3,2
TOTAL	**21,75*100**
DISSOLVED GAS PHASE	
Bubble point (bars)	12.7
Gas/liquid ratio (%)	14

Table 17 : site 6 - Particle and gas (bbp and GWR) measurements

DATE	11-Jul-13	11-Jul-13
SAMPLING POINT	PRODUCTION	PRODUCTION
OPERATING DATA		
Flow (m^3/h)	60-160	257
Pressure (bars)	1.5-3	3.0
Temperature (°C)	57.2	60.3
ELECTROCHEMICAL PARAMETERS		
pH brought back to 20°C	6.05	5.74
Potential Redox (mV)	-267	-311
Conductivity @ 20°C (µS/cm)	70,400	93,000
MAJOR IONIC PHASES (mg/l)		
Chloride	49,985	*
SUSPENDED PARTICLES	**mg/l * %**	**mg/l * %**
0,20 to 0,45 µm		1,590*1,5
0,45 to 1,20 µm	useless	37,386*35,2
1,20 to 3,00 µm	data	0,032*0,0
3,0 to 5,0 µm	-	25,821*24,3
5,0 to 8,0 µm	important	0,118*0,1
sup. of 8,0 µm	scaling	41,242*38,8
TOTAL		**106,19*100**
DISSOLVED GAS PHASE		
Bubble point (bars)	4.5	5.0
Gas/liquid ratio (%)	5	9

Table 18 : Fluid physical and thermodynamic properties

ITEM \ SITE	1	2	3	4	5	6	6
Wellhead temperature WHT (°C)	70	60	66	70	84	60	57
pH @ 20°C	6.08	6.45	6.07	6.25	5.84	5.74	6.01
Chloride Cl^- (mg/l)	77	62	68	78	84	-	50
Suspended particle concentration (mg/l)	42	16	22	114	24	106	-
Small particle (<0.45 µm) Concentration (% of total)	70	54	58	67	54	2	-
Bubble point BP (bar)	12.5	8.5	12.7	>1.4	>3.7	5.0	4.5
Gas liquid ratio GLR (%)	30	48	14	-	-	9	5

3.2.1. Electrochemical parameters

They address pHs (@20°C), Redox potentials and electrical conductivities (@20°C) and reflect the signature of an acid (pH#6) and saline (electrical conductivity #100.000-150.000 µS) geothermal brine.

3.2.2. Suspended particles

Total suspended solids concentrations evidence three categories, low (15-25 mg/l), medium (40-50 mg/l) and high (>100 mg/l) despectively of solid contents peaking on site 4. These solids may be internal particles entrained from the rock matrix by hydrodynamic forces or suspended particle precipitates of induced scale (carbonates, heavy metal sulfides, silica) species, most likely governed by CO_2 partial pressures and related degassing occurring below bubble point, or both. Mineralogic, qualitative (X Ray diffractometry) and quantitative (wet mode) analyses would obviously help in identifying such crytal particulates.

Particle of inframicrometric/colloidal sizes (diameters below 0.45 µm) prevail on all waters sampled in the western area, with proportions in excess of 50% of total solid contents, a distinctive attribute of such, fine gained sandstone hosted, fluids. They culminate on site 1 (70%) and site 4 (67%) doublets. By contrast, this ratio decreases to 2% on the site 6 doublets, carbonate reservoir fluids.

3.2.3. Bubble point and gas liquid ratio

Those critical parameters with respect to degassing and scale forming and growth could be reliably on five sites (site 1 via PVT analysis) the others – site 2 and 3 point/gas sampling device described in Figure .

On several sites these on the spot measurements could not be achieved due the presence of a degasser facility.

Of interest to note is the gas free operation of site 2 and 3 doublets as a result of surface equipments and facilities serviced above bubble point pressures, indeed a key issue in avoiding scaling shortcomings.

Gas (presumably methane dominant) liquid ratios remain below 50%.

Oil traces, known to affect at least two doublet localities, have not been detected during field measurements.

Again bottomhole fluid sampling and PVT analyses are strongly needed to precisely assess geothermal fluid thermochemistry.

3.3. Guidelines for improving well injectivity

A thorough assessment, taking into account sites specificities, of the well/near well formation damage – physical (internal particle entrainment), technological (well completion), thermochemical (CO_2 degassing, carbonate precipitation and scale), source mechanisms requires the following prerequisites:

- Well integrity: wireline log in section of casing/cement status
- Well/reservoir performance: production/injection well testing with bottomhole pressure (either wireline or slickline) recordings of build up/fall off cycles
- Bottomhole fluid sampling and PVT analyses (bubble point-degassing, pressure, gas liquid ratio, composition of the dissolved gaseous and separated liquid phases)
- Surface monitoring of suspended particles based on the, site specific, damage diagnosis and well status the following candidate means for improving injectivity could be implemented
- Higher production wellhead service pressures (implemented actually on doublets site 2 and site 3),
- Well stimulation using either organic (acetic, EDTA…) or mud (HCl + HF) acid formulations
- Submersible pump (ESP) vortex separator acting as an upstream pump degasser
- Downhole chemical injection line of properly formulated scaling inhibitors (a pilot test is presently underway on a fluid sampled downhole)
- Pressure sustained CO_2 injection (see development in section **3.7**)

3.4. Chemistry of geothermal waters

The scaling potential during the extraction of water from deep geothermal reservoirs depends foremost on the composition of the geothermal water itself. With the high dissolved contents that characterize these waters, also the potential for mineral precipitation increases. The extent, however to which this might occur, depends on the type and extent of physic-chemical changes that occurs with respect to the reservoir conditions from which the geothermal water was pumped. The most important changes that occur during the processing of geothermal water are the:

- temperature decrease during heat extraction (main purpose)
- total pressure decrease, as the geothermal water is pumped from great depths with high hydrostatic pressures (e.g. >200 bar at 2 000 m depth)

Here, we first focus on the composition of the various geothermal water analyzed, as it is the first factor that affects which and to what extent mineral precipitation might be induced by changes that in the process of geothermal heat extraction. Secondly, we address how water quality changes from production to injection, to address any noticeable changes that could indicate the occurrence of mineral precipitation or any other geochemical process that could lead to infectivity problems. Finally, we relate the various compositions of geothermal waters to the composition of accumulations for several of the geothermal systems studied.

3.4.1. Salinity

Sodium and chloride are the main constituents for all geothermal waters studied and their correlations are well correlated. The ratio between chloride and sodium indicates that their high salinities are mainly the result from the concentration of seawater. Only for site 1 is shifted closer to the ratio expected for halite (NaCl) dissolution. For all sites however, sodium and chloride concentrations are well below (>2x) those expected for halite equilibrium, even when cooled to a temperature of 30°C. Halite precipitation is therefore not expected to occur in any of the geothermal systems.

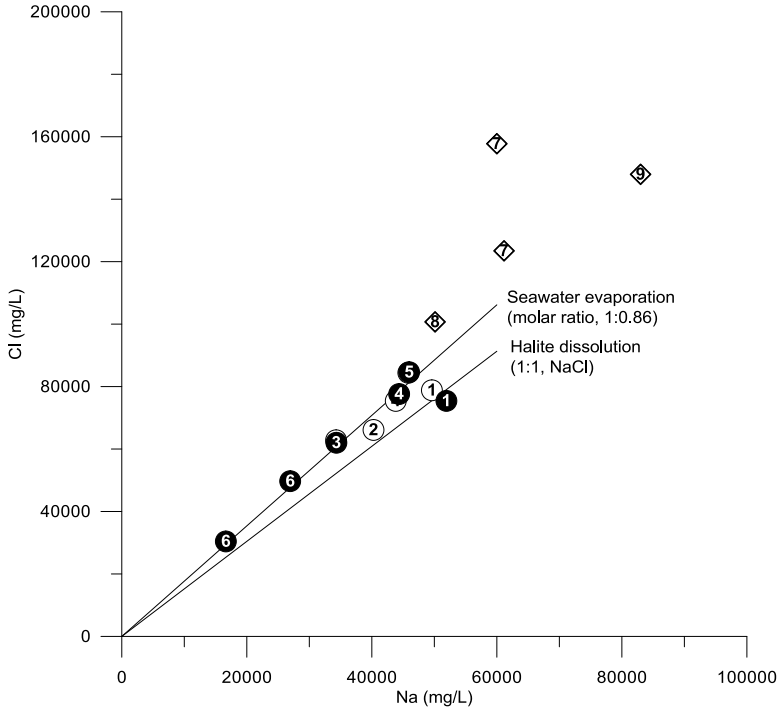

Figure 2: Sodium (Na) versus chloride (Cl) concentrations in the produced (black circles) waters for the studied sites

Numbers refer to the sites listed in Table 1. The diamonds indicate the compositions from the compilation by (Wasch 2014).

3.4.2. Gas compositions

The total amount and composition of gas dissolved in the geothermal waters is an important aspect with respect to pressure changes in the geothermal system. In the reservoir, the maximum amount of gas that can be dissolved is related to the total pressure in the reservoir. In the absence of over- or under pressure, this total pressure is equal to the hydrostatic pressure exerted by the height of the overlying water column. Therefore, with increasing depths, the hydrostatic pressure increases and for reservoir depths over 2 km, hydrostatic pressures and thus maximum dissolved gas pressure are over 200 atm. Whether or not the dissolved gas pressure equals the hydrostatic gas pressure depends on whether or not sufficient gas is available. In the presence of known free gas occurrences, this is surely the case. Typically, the above-ground geothermal system is operating under pressures that are at least multiple times lower (e.g. 15 atm) than the hydrostatic pressure from which the geothermal water is produced. Therefore it is expected that degassing occurs as the produced geothermal water is pumped upward along the pressure gradient. This is in keeping with the observations by GPC IP for the studied sites that the pressure in the production well had already dropped below the bubbling point (Ref. GPC IP), i.e. the gas pressure already exceeded the hydrostatic pressure in the upper part of the well and a free gas phase had already formed.

Degassing itself can cause clogging and injectivity problems, as reduction in water permeability occurs in the presence of free gas. The use of a degasser, will aid the prevention of gas clogging by removing the amount of free gas that is produced by the time the produced water reaches the surface operation. However, in the formation and removal of free gas the potential for the precipitation of carbonate minerals is induced, following for the precipitation of calcite ($CaCO_3$):

$$Ca^{2+} + 2\ HCO_3^- = CaCO_3(s) + CO_2(g) + H2O(l)$$

where HCO_3- is measured as alkalinity (or acid buffering capacity) and the subscripts s, g and l refer to the formation of solid, gas and liquid phases. The extent to which carbonate minerals precipitate therefore depends on extent to which CO_2 is removed during degassing, which in turn depends on the partial pressure of CO_2 in the reservoir. This partial pressure is a function of the molar (~volumetric) fraction of CO_2 in the gas and the total gas pressure in the reservoir.

Results of the analyses on the gas contained in the produced water (Figure), indicate that methane (CH_4) is the major component (>85%) in the dissolved gas phase for sites 1, 3 and 4. For site 5 and particularly site 6 the methane fraction is lower at 75% and 25% respectively. For the methane rich samples, CO_2 represent the second-largest fraction (few percent) of the remaining gasses present. Overall, these gas compositions fall well within the range of the majority of gas compositions measured during gas- and oil exploration (nlog.nl).

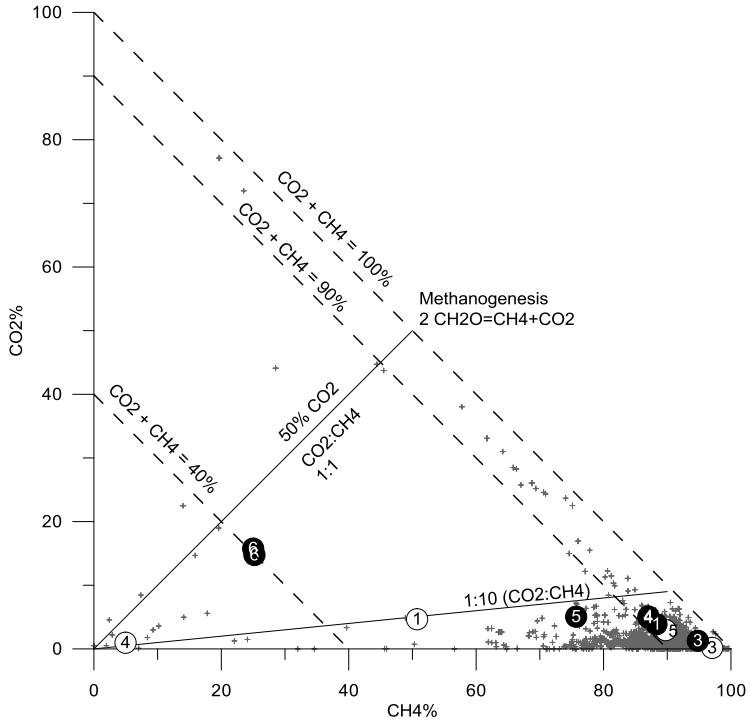

Figure 3: Relative proportions of methane (CH4) versus carbon dioxide (CO2) in the total amount of gas extracted from geothermal waters

Numbers refer to the sites as listed in Table 1. Black circles refer to the compositions in the produced water, white circles refer to the composition in the injected water. For reference, the grey plusses indicate gas compositions measured for Dutch oil and gas production (nlog.nl).

The determined dissolved gas composition for the produced water at site 6 has a relatively low carbon dioxide and methane fraction. Due to the relatively low gas content in the produced water at site 6 location, the content of gases other than CO_2 and CH_4 could not be determined. However, in contrast with the produced water in the other sites, the near equal content for these two species would be indicative a methanogenic contribution rather than a thermogenic origin of the methane. This is also, supported by the relatively low ethane fraction (Figure). In contrast, the relatively high ethane fraction for particularly site 1 indicates the presence of a "wet gas" with oil related compounds.

Strikingly, the relative methane fractions were strongly reduced in the injection water for site 1 and 4, both sites that operate a degasser. For typical gas compositions, the predominant fractions besides methane and CO_2 is nitrogen (N_2). Nitrogen however, accounted only for 31% and 3.9% of the total gas composition. After switching the carrier gas of the GC to argon, it was verified that in addition to nitrogen, helium contributed to 22% and 88% of the gas phase. The strong increase in the percentage of helium in the injection water for these geothermal systems, is attributed to the relatively low gas pressure remaining in the water after degassing. Since helium has a very high Henry's constant, this results in preferential loss of helium from the sampled water when partitioning with the headspace during extraction. Therefore, for these two sites, it is expected that fractionation during gas sampling resulted in an overestimation of the most volatile gasses such as particularly helium. To a lesser extent, this is also reflected in the relative increase of methane compared to ethane in the injection waters for sites 1, 4 and 5 (Figure).

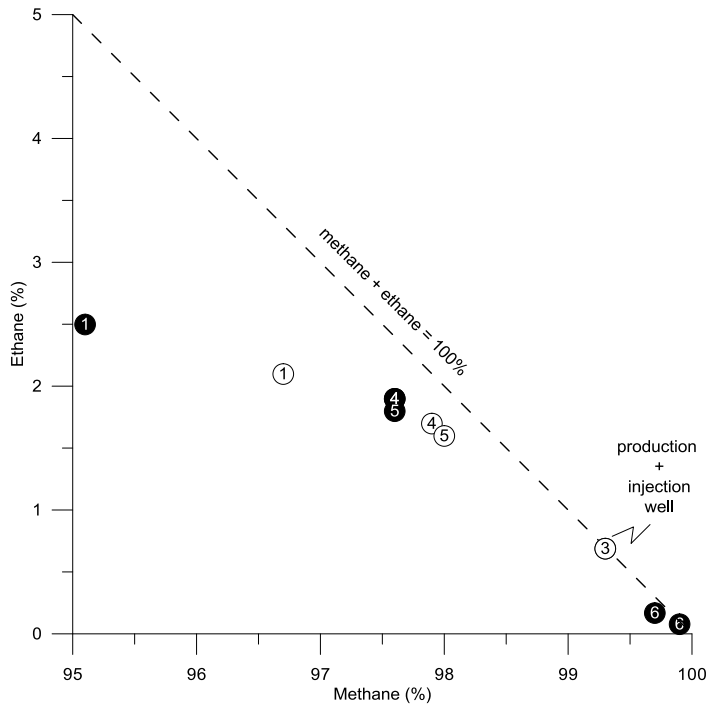

Figure 4: Relative proportions of methane (CH4) versus ethane as a fraction of the total organic components (C1-C6+) in the gas extracted from geothermal waters

Numbers refer to the sites as listed in Table 1. Black circles refer to the compositions in the produced water, white circles refer to the composition in the injected water.

3.4.3. Carbonate vs CO_2 equilibria

The amount of carbonate that can precipitate due to CO_2 degassing depends on the alkalinity and the concentration of available cations to form a carbonate phase. Unlike most common minerals, carbonates are more soluble with lower temperatures. This is illustrated when comparing the modelled calcite solubilities for different temperatures at identical CO_2 pressures (Figure 6). Therefore, cooling would act to decrease the scaling potential induced by CO_2 degassing. A noteworthy exception is however the lead mineral cerrusite, a carbonate ($PbCO_3$) which solubility does decrease with decreasing temperatures (http://thermoddem.brgm.fr).

The geothermal water analysed are relatively rich in calcium compared to alkalinity, as are many other Dutch reservoirs as illustrated by the data from (Verweij 2003). This means that stoichiometrically, there is sufficient calcium present to precipitate all alkalinity as calcite ($CaCO_3$). Since alkalinity is limiting the potential for calcite precipitation, site 6, with the highest alkalinity is the geothermal system with the highest calcite precipitation potential. However, the extent to which various carbonate minerals, or more likely, mixtures thereof, depends strongly on the rate with which they precipitate. This favours the precipitation of less soluble carbonates such as iron or lead carbonates, if sufficient concentrations of these cations are available for precipitation.

As discussed in the previous section, CO_2 only represents only a small fraction of the total gas pressure. However, for a hydrostatic pressure in the originating reservoir of 200atm, a CO_2 percentage of 1 percent of the total dissolved gasses results in a partial CO_2 pressure of 2 atm. Although for sites the total gas pressure could not be determined using the bubble point method (REF GPC), the partial CO_2 pressure can estimated when assuming calcite equilibrium in the reservoirs (Figure 5). This suggests the highest partial CO_2 pressure for site 6 of around 3 to 4 atm. For the other sites, partial CO_2 pressures below 1.5atm are estimated. This is similar to the range of partial CO_2 pressures estimated for hydrostatic pressures of over 200atm for the reservoir depths over 2km and the CO_2 gas fractions of 1 to 4% for the produced water at these sites (Figure 3).

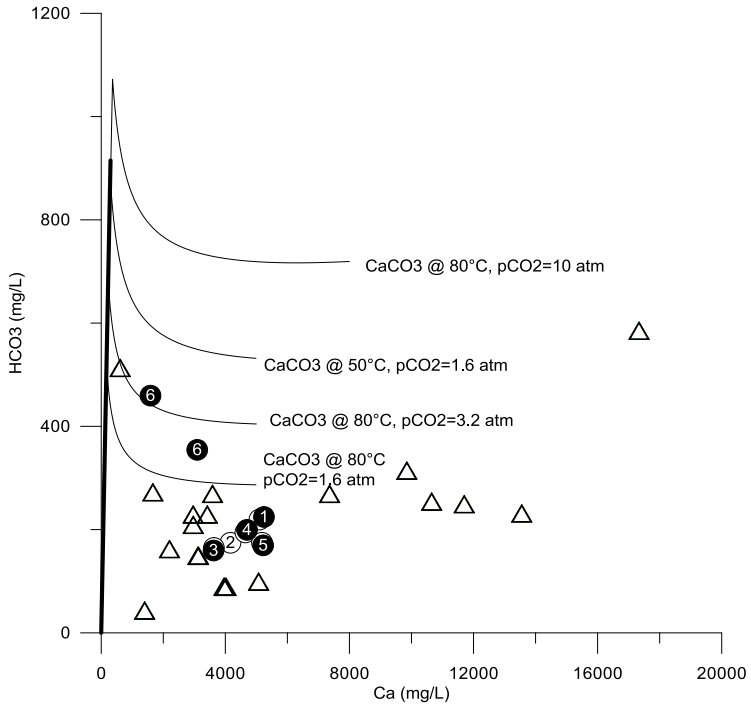

Figure 5: Calcium (Ca) and alkalinity (HCO3) concentrations for the sites studied

Numbers refer to the sites as listed in Table 1. Black circles refer to the compositions in the produced water, white circles refer to the composition in the injected water. Triangles indicate measurements in various Dutch reservoirs (Verweijk 2003). The lines are equilibrium scenarios for different partial CO2 pressures and temperatures as modelled using PHREEQC. The bold black line represents the stoichiometric ration along which calcite would precipitate due to CO2 degassing.

3.4.4. Barite supersaturation

V In addition to carbonate minerals, the precipitation of barite (BaSO4) was identified as an additional potential for scaling (Figure 6), with the highest potential observed for site 4. However, modeling indicates that the solutions 100 (SI=2) to 1000 (SI=3) times supersaturated with respect to the theoretical solubility product of barite, as are various Dutch reservoirs (Verweij 2003). This indicates that barite precipitation is inhibited in these geothermal reservoirs, possibly because of brine composition. If the barite does not precipitate from the geothermal water in the reservoir at such high supersaturations, there is little reason to assume that barite would precipitate in the geothermal system after production, particularly as the temperature decline has only a limited effect on the degree of supersaturation.

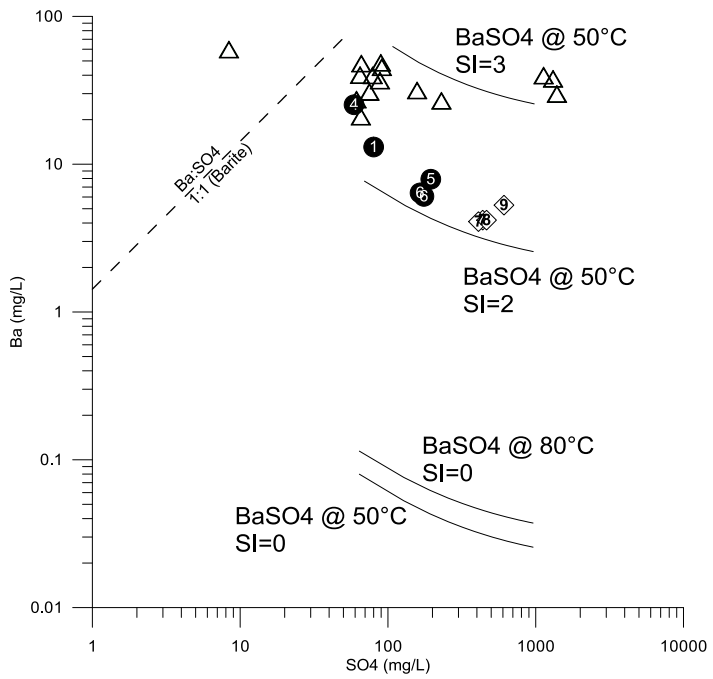

Figure 6: Barium (Ba) and sulphate (SO4) concentrations for the sites studied. Numbers refer to the sites as listed in Table 1

Black circles refer to the compositions in the produced water. Triangles indicate measurements in various Dutch reservoirs (Verweij 2003). indicate the compositions from the compilation by (Wasch 2014). The lines are equilibrium scenarios for different temperatures and saturation indices (SI) as modelled using PHREEQC. The SI values represent the log value of the solubility product divided by the equilibrium constant. The dashed line represents the stoichiometric ration along which barite would precipitate (or dissolve).

3.5. Scaling composition

In the four accumulations analysed, the most abundant elements (Table 19) are calcium for site 1, iron for site 5 and lead for site 7. The lack of silicium or barium enrichments confirms the insignificance of silica or barite precipitation. Besides the absolute abundance, the relative increase of elements in the composition of the accumulates with respect to that of the produced water, indicates the preferential concentration of that element as would be expected for mineral precipitates. For all four accumulates analysed, lead and iron were concentrated with respect to calcium in comparison to their produced water composition by an average factor of 100,000
(Figure) and 50 (Figure) respectively. This is indicative of the preferential precipitation of the less soluble lead and iron carbonates relative to calcium carbonate (calcite).

Table 19: The 7 highest elements determined in the accumulations analysed

Rank	Site 1 Scalant		Site 1 Filter		Site 5 Filter		Site 7 Scalant	
	Element	wt. %	Element	wt. %	Element	wt. %	Element	wt. %
1	Ca	19,7	Ca	14,1	Fe	18,8	Pb	56,1
2	Fe	3,2	Fe	11,1	Cl	5,6	Cl	4,0
3	SO4	2,2	SO4	2,2	Na	3,4	Na	2,2
4	Cl	0,5	Cl	1,2	Mn	1,9	Ca	1,3
5	Mg	0,5	Na	0,7	SO4	1,7	Fe	0,9
6	Na	0,3	Mg	0,4	Ca	0,5	SO4	0,1
7	Sr	0,2	Mn	0,3	Pb	0,5	Mg	0,1

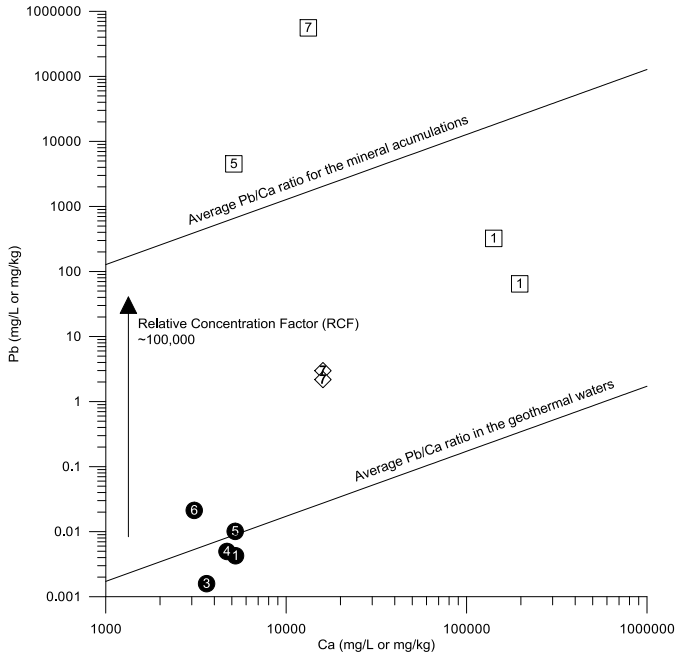

Figure 7: Calcium (Ca) and lead (Pb) concentrations of produced water and accumulates at the sites studied

Black circles refer to the compositions in the produced water in mg/L. Squares indicate the concentrations in the accumulations in mg/kg. Numbers refer to the sites as listed in Table 1. Diamonds indicate the compositions of produced water from the compilation by (Wasch 2014). The lines are the through-the-origin fits, representing the average Pb/Ca ratios for the produced water and accumulates.

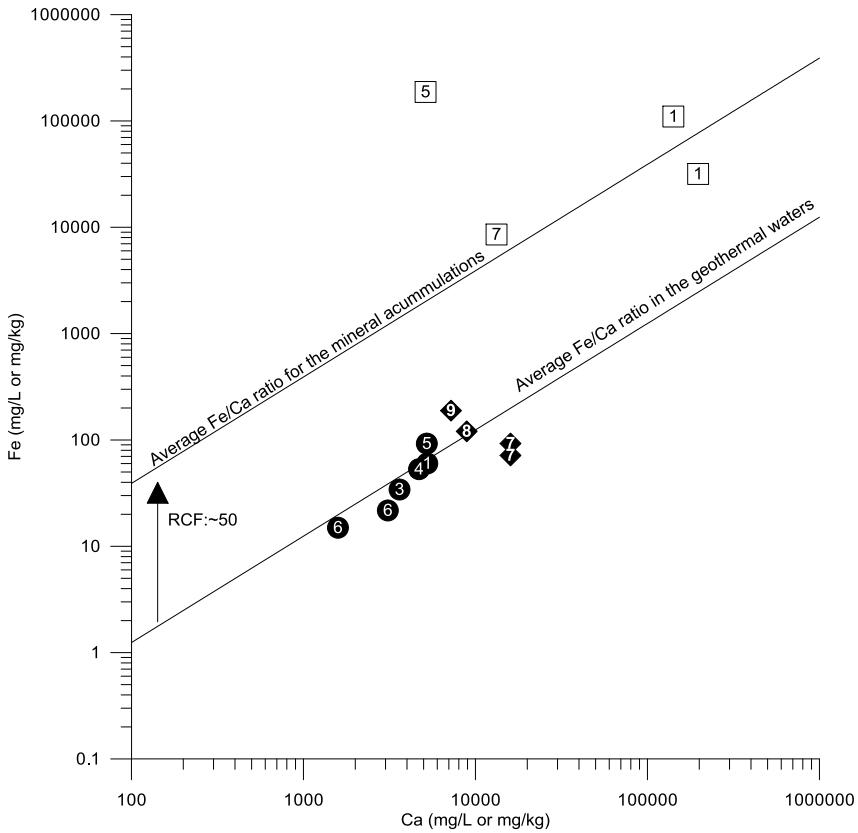

Figure 8: Calcium (Ca) and iron (Fe) concentrations of produced water and accumulates at the sites studied

Black circles refer to the compositions in the produced water in mg/L. Squares indicate the concentrations in the accumulations in mg/kg. Numbers refer to the sites as listed in Table 1. Diamonds indicate the compositions of produced water from the compilation by (Wasch 2014). The lines are the through-the-origin fits, representing the average Fe/Ca ratios for the produced water and accumulates.

The analysed accumulates were to various extents saturated with brine, which explains the relatively high chloride contents. Using the measured chloride concentration in the accumulates with the corresponding produced water composition allowed estimation of the residual brine water content (Table 20). Although this water content also fully explained the measured sodium concentrations, sulphate concentrations are enhanced relative to the concentrations based on brine water composition for the accumulates of site 1 and 5, indicating a minor contribution of sulphate precipitation. Overall, however, the precipitates appear to be dominated by the precipitation of carbonate phases, as was confirmed when conducting an acid test on the accumulates to verify the dissolution of the accumulate and the production of gas (CO_2), following:

$$CaCO_3 + 2H^+ = Ca^{2+} + CO_2(g) + H_2O$$

While the observed effervescence was high (+) to very high (++) for the site 1 and site 7 accumulates (Table 20), it was low (-) for the Fe-rich GW accumulate. This is in keeping with the known low dissolution rate of iron carbonates in acid [e.g. (Hartog 2003)].

Table 20: Overall characterization of the accumulates analysed

Site	Type	Water %	Aci Test	Residue		Carbonate phase	
				Present	Aceton solvable	Main	Minor
1	Scalant Filter	7.4 17.3	+ +	yes yes	yes yes	$CaCO_3$ $CaCO_3$	$FeCO_3$ $FeCO_3$
5	Filter	72,1	-	yes	yes	$FeCO_3$	$MnCO_3$
7	Scalant	35,2	++	no	-	$PbCO_3$	$CaCO_3$

The residual brine water content dilutes the elemental abundancies in the overall analysis of the accumulate composition largely with sodium and chloride (Table 19), particularly for the site 5 and site 7 samples. The consideration of this residual brine water content (Table 20), indicates that the carbonate phases are indeed the main component of the accumulations studied. For site 1 the accumulations consists of mixture of mainly Ca-carbonate mixed with Fe-carbonate (Table 20), while for site 5 the carbonate phase is predominantly Fe-carbonate with probably minor contributions of Mn-carbonates. The carbonate precipitate from site 7 largely consists of Pb-carbonate with only minute contributions by Ca and Fe. It is unlikely that metallic lead contributed to the total lead content, as there was no residue following the acid test. However, metallic lead is a known scaling from gas production facilities in the Slochteren reservoir (Schmidt 2000Schmidt 2000). The potential to form this scale results from the production of lead containing reservoir water. Rather than direct steel corrosion by dissolved lead, corrosion by the degassing induced precipitation of Pb-carbonate scaling might result at the steel-precipitate interface as follows:

$$Fe^0 + PbCO_3 = FeCO_3 + Pb^0$$

Expectedly, this would result in elevated iron fractions in the carbonate phase, which were not observed (Table 19). Also, since no residue was detected after removing all carbonates with the acid test (Table 20), no significant amounts of metallic lead were present in the analysed accumulate from site 7.

In contrast with the accumulate from site 7, the accumulates from sites 1 and 5 did yield residues after dissolution of all carbonates with the acid test (Table 20). The residues represented less than a few percent of the initial accumulate mass. The fact that these residues did not dissolve in water or acid, but did readily dissolve in Aceton, indicates that these residues are organic, probably oil-related, in nature. The exact nature and extent which these hydrophobic components might contribute to injectivity problems is not yet clear.

3.6. Impact of water quality changes on formation of mineral precipitates

The comparison of produced and injected water compositions appears as a straightforward approach to addressing the geochemical processes that occur in the geothermal system. However, since the geothermal systems are operating with high flow rates (e.g. 100-200 m^3/hr) even very small compositional changes can result in the build of precipitates and injectivity problems. Therefore, reaction rates must be sufficiently high to be able to monitor quality differences between produced and injected water.

Particularly, for the process of degassing these rates appear to be very high. Degassing already occurred in the production wells (see **§3.1**) before the point where the production water could be sampled. Also observed in the production well is the presence of many small particles (see **§3.2.2**). These particles are likely carbonate particles that are formed as a result of the loss of CO2 pressure that occurs with degassing, as described in section **3.4.3** to distinguish between dissolved and particulate solids, the commonly used, operationally defined exclusion size of 0.45 µm was used for filtration. Since a large fraction of the produced particles measured (see **§3.2.2**) were smaller, a strict isolation of dissolved concentrations turned out not to be possible.

To test whether the extent to which the filtration of samples removed particles, all water samples were additionally analysed without filtration. Overall, the differences between the composition of filtered and unfiltered, and produced and injected water was very small. This can be explained when a large fraction of the particles formed during production and in the geothermal system were not separated by filtration. Small differences between filtered and unfiltered water were however observed for some elements (Figure). Filtration seems to impact calcium concentrations more than iron concentrations. This is however not conclusive, since this could either be the result of less Fe-carbonate particle formation or by a generally smaller particle for Fe-rich carbonate particles compared to Ca-rich carbonate particles. However, since the difference between filtered and unfiltered water is larger for the injection water, this suggests that iron-rich carbonate particles are formed later than the Fe-rich carbonate particles. Also, the largest difference in calcium concentrations for site 1 and the absence thereof for site 5, is in keeping with the relative importance of calcium carbonates in the analysed accumulations for these sites (Table 20).

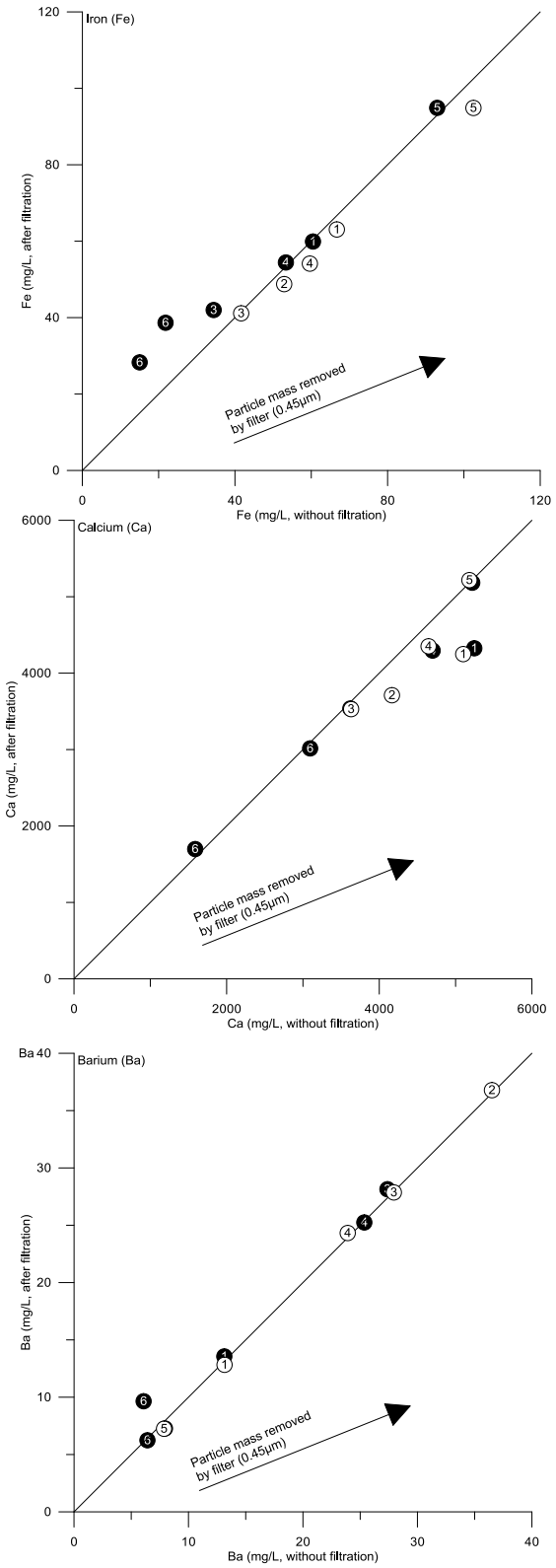

Figure 9: Comparison of measured concentrations for iron, calcium and barium, with and without filtration over a 0.45 µm filter

Numbers refer to the sites as listed in Table 1. Black circles refer to the compositions in the produced water, white circles refer to the composition in the injected water.

3.7. A step-wise approach towards improving injectivity

Based on the geochemical analysis of the production waters and accumulations from several of the geothermal systems, carbonate precipitation due to degassing of CO_2 appears to be the foremost factor causing scaling and injectivity problems. The cooling that occurs through the extraction of heat is not expected to increase the precipitation potential as most of the carbonates are more soluble at lower temperatures. Only where the precipitation of lead carbonate dominant (such as for site 7), lower injection temperatures are likely to lead to additional precipitation.

Preventing degassing altogether is not a feasible strategy if it would require the surface installation to operate under the much higher pressures of the reservoir (e.g. >200atm for a reservoir depth at 2km). Therefore, the use of a degasser in a geothermal system aids in preventing the formation of free gas and potential gas clogging further on. However, since degassing of CO_2 pressure acts as the main driver for the carbonate precipitation observed, CO_2 pressure control also provides the main key to its prevention. Luckily, CO_2 appears to only represent a small fraction of the total gas pressure in the geothermal reservoirs studied (Figure). And in principle, it is only this partial CO_2 pressure that would need to be maintained or restored to prevent or re-dissolve carbonate precipitation. Recent field applications of CO2-dosing during RO (reverse osmosis) concentrate injections have have illustrated its effectiveness to prevent carbonate scaling in both the well screen and the target aquifer. A short description of the experience with the application of CO2-dosing is provided in Highlight 1. For sites with lead carbonate precipitation, an increased CO_2 pressure is required to compensate for the decrease of lead carbonate solubility with lower temperatures.

For the geothermal sites studied, the highest partial CO_2 pressure is derived for site 6 at 3-4 atm. This pressure is well below the typical operational pressure under which the surface part of geothermal systems are typically maintained (10-20atm). These operational pressures are therefore sufficiently high to allow the addition of sufficient CO_2 to restore the partial CO_2 pressure of the reservoir, while keeping all added CO_2 dissolved throughout the system. For the re-dissolution of a carbonate mineral:

$$XCO_3(s) + CO_2(g) + H_2O(l) = X^{2+} + 2\ HCO_3^-$$

Where X can be any divalent cation (Ca, Pb, Fe, Mn, etc).

Based on this study, the following steps-wise approach to improving injectivity for a geothermal site is proposed:

1. Establish how CO_2 dosing would be best integrated, taking into account the various operational aspects (degasser, operational pressure, injection pressure and temperature)
2. Optimize CO_2-dosing based on the site-specific partial CO_2 pressure and type of carbonate precipitate to prevent precipitating or enable re-dissolving them again.
3. The use of hydrochloric acid dosing can be considered as a faster, more aggressive method to restore injectivity after which injection with CO_2 dosing can maintain injectivity. Since acid treatment of carbonates results itself in CO_2 production, care has to be taken not to generate CO_2 quantities beyond the pressures maintained during operation.
4. The use of surfactants can be considered. These typically aid in keeping cations in solutions, but are however hard to target specifically the cations that are involved with the precipitation of the carbonate phases. Therefore the use of these type of inhibitors requires significant overdosing. Also, the effectiveness of these inhibitors is likely limited once particles have already precipitated in the system, e.g. in the production well. However, surfactant use seems to be suitable for target purposes, such as the prevention of scaling of the heat exchanger, for particular minerals that lower solubilities at lower temperatures.
5. Beyond the precipitation of carbonates, results indicate the formation of oil residues in scaling and on filters (Table 20). For now, it is uncertain to what extent these oil residues also contribute to some of the injectivity problems. This would require further study, which in part will become clear once the prevention of carbonate precipitation is appropriately addressed.

Highlight 1:

CO_2 dosing as a measure to prevent carbonate clogging at a BWRO injection well

Brackish groundwater may serve as a source for drinking and irrigation water, after desalination with low-pressure reverse osmosis membranes (brackish water reverse osmosis, BWRO). Besides the fresh water permeate, a flow of membrane concentrate is produced. The increase in salinity of this concentrate with respect to the original brackish groundwater depends on the recovery with which the RO is operated. Deep well injection into a (more) saline, confined aquifer allows the disposal of the concentrate without burdening surface waters.

As RO results in the concentration of all dissolved salts in the concentrate, the concentrate is supersaturated with respect to various minerals, depending on the recovery at which an RO system operates. With an RO recovery of 50% concentrations are increased two-fold, with 65% three-fold. Therefore, a technical risk of BWRO concentrate injection is clogging of the injection well and receiving aquifer with mineral precipitates, particularly carbonates.

For a particular RO research pilot, pressures were monitored in detail (see figure) at the injection well (blue line) and in the aquifer (purple line) during concentrate injection. During phase A a recovery of 50% was maintained with an injection rate of 25m^3/hr. After recovery was increased in Phase B to 65% with an injection rate of 17.5 m^3/hr, the injection well started clogging and increased injection pressures (from 3 to 5 bar) were required to maintain the injection rate. Calcite precipitation was the dominant cause of this well clogging, as deduced from monitoring data in the injection aquifer. Treatment with HCl only partly regenerated the well, after which recovery was reduced to 50%. Only with the dosing of CO_2 to prevent carbonate supersaturation in Phase F, recovery could be maintained at 65%, with no loss in injectivity, as indicated by the constant and stable injection pressures at stage F of the experiment.

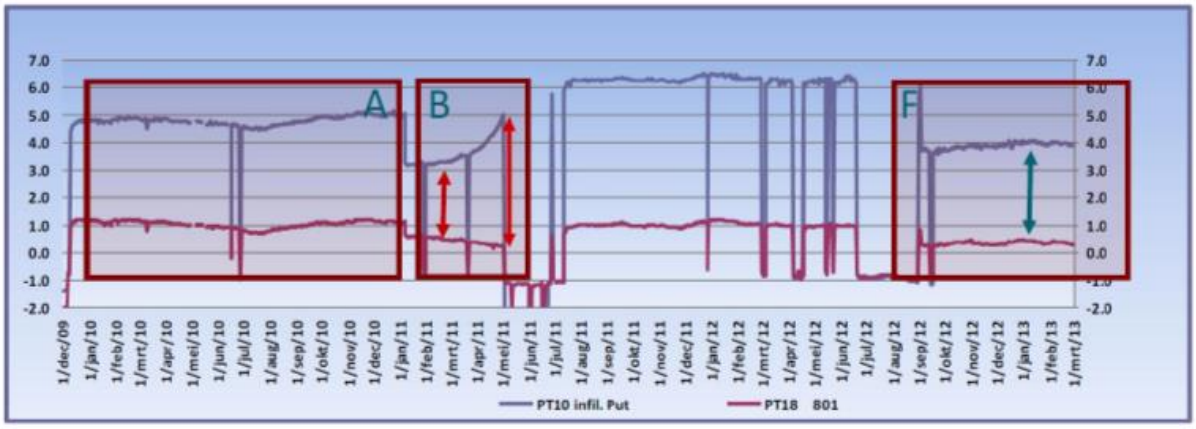

Injection pressure at BWRO injection well at various stages of the pilot. A = 50% recovery; B = 65% recovery (increasing pressure indicates clogging); F = 65% recovery + CO_2 dosing.

4. CONCLUSIONS. RECOMMENDATIONS

An extensive measurement campaign consisting in water and gas sampling, electrical measurements, doublet diagnosis has been carried out in July 2013 with a view to identify the causes of poor well injectivities. This research programme has been implemented jointly by GPC IP and KWR. Within this research, GPC IP investigations concentrated on well performance and fluid physical and thermodynamic properties, while KWR concerns focused on the geochemical processes occuring in geothermal systems and deemed decisive in the damaging process.

The main problems identified on most of the sites are low pumping efficiencies, degassing and scaling. In some instances the degassing occurs right in the well and two phase flow is observed.

Further to the analysis of gases and scale samples it is clear that one of the main responsible for the existence of high quantities of particles in the geothermal loop is the degassing of CO_2 which leads for instance to the precipitation of carbonates. On one site important quantities of lead carbonates were assessed.

It is concluded that the main cause for accumulation of minerals on filters and as scaling is due to the degassing of CO_2 during the rise in the production well and in subsequent parts of the geothermal system. The CO_2 degassing results from the drop in the gas pressure that is maintained at reservoir depth (hydrostatic pressure) to the relatively low pressure at which the geothermal system at the surface are operated. The loss of CO_2 results in subsequent precipitation of carbonate minerals.

Depending on the chemical composition of the geothermal water in the reservoir, Ca-rich, Fe-rich or Pb-rich carbonates were preferentially precipitated, as was confirmed by analysis of filter and scaling accumulates from various systems.

Among the candidate remedial alternatives, to be implemented further to a thorough-site specific-damage diagnosis and well status, ought to be mentioned:

(i) higher (above bubble point) production wellhead pressures whenever allowed by heat exchanger service pressures, as practiced actually on the site 2 and 3 doublets;

(ii) well stimulation using either organic (acetic, EDTA...) or mud (HCl + HF) acids;

(iii) submersible pump (ESP) vortex separators;

(iv) downhole chemical injection lines of scaling inhibitors, designed further to pilot tests on geothermal fluids sampled downhole, and

(v) last but not least pressure sustained $C0_2$ injection. Actually, since degassing of CO_2 pressure acts as the main driver for the carbonate precipitation observed, CO_2 pressure control also provides a solution. Luckily, since CO_2 appears to only represent a relatively small fraction of the total gas pressure in the geothermal reservoirs studied, only a limited level of CO_2-dosing is required to prevent or re-dissolve carbonate precipitates. The required partial CO_2 pressure seems well achievable within the operational pressures currently maintained in the geothermal systems. For sites with lead carbonate precipitation, an increased CO_2 pressure is required to compensate for the decrease of lead carbonate solubility with lower temperatures.

There is no standard solution for the injection problems of all the wells, each site shall be treated individually.

REFERENCES:

Borozdina; O., Ratouis, T., Ungemach, P. and Antics, M. (2013). Thermochemical impact of cooled brine injection. Paper presented at the European Geothermal Congress, **EGC 2013**, Pisa, Italy, 3-7 June, 2013.

Hartog, N. (2003). Reactivity of organic matter and other reductants in aquifer sediments, Utrecht University.

Schmidt, A. P. (2000). Naturally occurring radioactive materials in the gas and oil industry: origin, transport and deposition of stable lead and 210Pb from Dutch gas reservoirs, Universiteit Utrecht.

Ungemach, P. (2003): Reinjection of cooled geothermal brines into sandstone reservoirs. *Geothermics*, **32**, 743-761

Verweij, J. M. (2003). Fluid Flow Systems Analysis on Geological Timescales in Onshore and Offshore Netherlands: With Special Reference to the Broad Fourteens Basin, Netherlands Institute of Applied Geoscience TNO, National Geological Survey.

Wasch, L. J. (2014). Geothermal energy – Scaling potential with cooling and CO2 degassing, TNO: 22.

Authors:

Miklos Antics:

- GPC Instrumentation Process / Geofluid
- PARIS NORD II – Immeuble Business Park – Batiment 4A
- 165, Rue de la Belle Etoille – B.P. 55030
- 95946 Roissy CDG CEDEX
- office@geoproduction.fr

Niels Hartog :

- KWR Watercycle Research Institute
- Groningenhaven 7
- 3433 PE Nieuwegein
- info@kwrwater.nl